

## P- and S-wave simulation using a Cole–Cole model to incorporate thermoelastic attenuation and dispersion

José M. Carcione,<sup>1,2</sup> Stefano Picotti,<sup>2</sup> and Jing Ba<sup>1,a)</sup>

<sup>1</sup>*School of Earth Sciences and Engineering, Hohai University, Nanjing, China*

<sup>2</sup>*National Institute of Oceanography and Applied Geophysics–OGS, Borgo Grotta Gigante 42c, 34010 Sgonico, Trieste, Italy*

### ABSTRACT:

In thermoelastic wave attenuation, such as that caused by heterogeneities much smaller than the wavelength, e.g., Savage theory of spherical pores, the shape of the relaxation peak differs from that of the Zener (or standard linear solid) mechanical model. In these effective homogeneous media, the anelastic behavior is better represented by a stress-strain relation based on fractional derivatives; particularly, P- and S-wave dispersion and attenuation is well described by a Cole–Cole equation. We propose a time-domain algorithm for wave propagation based on the Grünwald–Letnikov numerical derivative and the Fourier pseudospectral method to compute the spatial derivatives. As an example, we consider Savage theory and verify the algorithm by comparison with the analytical solution in homogeneous media based on the frequency-domain Green function. Moreover, we illustrate the modeling performance with wave propagation in a two half-space medium where one section is lossless and the other is a Cole–Cole medium. This apparently simple example, which does not have an analytical solution, shows the complexity of the wavefield that characterizes a single flat interface. © 2021 Acoustical Society of America.

<https://doi.org/10.1121/10.0003749>

(Received 23 October 2020; revised 2 February 2021; accepted 22 February 2021; published online 22 March 2021)

[Editor: Nickolas Vlahopoulos]

Pages: 1946–1954

### I. INTRODUCTION

Heat flow is one of the mechanisms to explain anelastic wave propagation (Savage, 1966; Treitel, 1959; Zener, 1938). Heterogeneities and/or cracks or cavities much smaller than the signal wavelength affect the compressional (P) and shear (S) waves by dissipating their energy to heat. Zener (1938) explained the physics in these terms: “Stress inhomogeneities in a vibrating body give rise to fluctuations in temperature, and hence to local heat currents. These heat currents increase the entropy of the vibrating solid, and hence are a source of internal friction.” Mechanical and heat sources induce temperature gradients, and the flow or diffusion equalizes the temperature difference and gives rise to P- and S-wave energy dissipation and velocity dispersion. This physical mechanism is the basis of thermoelasticity or non-isothermal elasticity (Carcione *et al.*, 2019b; Carcione *et al.*, 2020a; Carcione *et al.*, 2019c; Lord and Shulman, 1967). A similar phenomenon occurs in poroelasticity, where the Biot slow mode represents energy loss (attenuation) due to fluid-pressure diffusion (Carcione *et al.*, 2019b; Picotti and Carcione, 2017).

In Carcione *et al.* (2020a), we present analytical solutions of thermoelasticity, related to the attenuation and dispersion of the P and S waves and not algorithms to simulate wave propagation. On the other hand, Carcione *et al.* (2020b) deals with the simulation of P waves. Here, we generalize this thermo-acoustic approach to simulate P and S waves with the

Cole–Cole stress-strain relation [Cole and Cole (1941) and Eq. (8.138) of Carcione (2014)]. This rheology requires the use of fractional time derivatives. Many authors used fractional calculus as an empirical tool to describe the properties of linear viscoelastic materials (Caputo, 1967; Caputo and Mainardi, 1971), and a wide bibliography is given in Mainardi (2010), including a historical perspective. A quite recent overview of these topics is provided in Holm (2019).

There are several works where the Cole–Cole model is analyzed, but many of these works denote this model as the fractional Zener model instead of the Cole–Cole. In-depth analyses are provided for attenuation and dispersion properties and power-law regimes for Cole–Cole/fractional Zener viscoelastic media (Chandrasekaran and Holm, 2019; Näsholm, 2013; Näsholm and Holm, 2013; Parker *et al.*, 2019; Wismer, 2006). The related wave equations are also developed under assumptions of linear conservations of momentum and mass. Fractional calculus has been applied in thermoelasticity, mostly based on the Caputo derivative (e.g., Garra, 2017), which is an analytical tool to solve fractional differential equations. The Cole–Cole model, originally adopted for an optimal fit of electromagnetic experimental data (Cole and Cole, 1941), has been used in different works to describe wave attenuation (e.g., Spencer, 1981; Picotti and Carcione, 2017).

We propose to solve the time-domain differential equations with a direct grid method, where the spatial derivatives are computed with the Fourier pseudospectral method (e.g., Carcione, 2014) and the fractional time derivatives with the Grünwald–Letnikov (GL) series (Caputo *et al.*, 2011;

<sup>a)</sup>Electronic mail: [jingba@188.com](mailto:jingba@188.com)

Carcione *et al.*, 2002), which is an extension of the standard finite-difference approximation for derivatives of integer order. As an example, we consider the theory proposed by Savage (1966) for empty round pores. In this model, the P and S waves suffer attenuation due to shear loss, while there are no losses due to dilatational deformations.

II. THE COLE-COLE MODEL

Effective attenuation can be described by means of power laws in the form of fractional derivatives. With the purpose of obtaining the equivalent viscoelastic medium, we use the Cole-Cole model, which has been adopted to describe dispersion and energy loss (attenuation) in dielectrics, anelastic media, and electric networks (Bagley and Torvik, 1986; Bano, 2004; Cole and Cole, 1941; Grimnes and Martinsen, 2005; Hanyga, 2003). The frequency-domain Cole-Cole stress-strain relation (based on irrational powers of the frequency) can be represented in the time domain as a differential equation involving derivatives of fractional order (e.g., Carcione, 2014). The complex modulus of a Cole-Cole element can be expressed as

$$M(\omega) = M_R \cdot \frac{1 + (i\omega\tau_\epsilon)^q}{1 + (i\omega\tau_\sigma)^q}, \tag{1}$$

where  $\omega$  is the angular frequency,  $M_R$  is the relaxed (low-frequency) modulus,  $\tau_\sigma$  and  $\tau_\epsilon$  are relaxation times,  $0 \leq q < 2$  is a real number, and  $i = \sqrt{-1}$  is the imaginary number. When  $q = 1$ , we obtain the Zener model (e.g., Carcione, 2014), while  $q = 0$  gives the lossless case. The quality factor associated with  $M$  is  $\text{Re}(M)/\text{Im}(M)$ , where  $\text{Re}$  and  $\text{Im}$  denote real and imaginary parts, respectively. Its minimum value is located at

$$\omega_0 = \frac{1}{\sqrt{\tau_\sigma\tau_\epsilon}} \tag{2}$$

and is equal to

$$Q_0 = \frac{(1 + \gamma^2)\cot \varphi + 2\gamma \csc \varphi}{\gamma^2 - 1},$$

$$\gamma = \left(\frac{\tau_\epsilon}{\tau_\sigma}\right)^{q/2}, \quad \varphi = \frac{\pi q}{2}. \tag{3}$$

$f_0 = \omega_0/(2\pi)$  is the central frequency of the relaxation peak, and  $1/Q_0$  is the maximum dissipation factor (e.g., Carcione, 2014).

Using  $\omega_0$  and  $Q_0$  as parameters, we have

$$\tau_\epsilon = \frac{\gamma^{1/q}}{\omega_0}, \quad \tau_\sigma = \frac{\gamma^{-1/q}}{\omega_0}, \tag{4}$$

where  $\gamma$  is a solution of Eq. (3):

$$\gamma = \frac{1 + \sqrt{1 + Q_0^2} \sin \varphi}{Q_0 \sin \varphi - \cos \varphi}. \tag{5}$$

The unrelaxed (high-frequency) modulus is

$$M_U = M_R \left(\frac{\tau_\epsilon}{\tau_\sigma}\right)^q. \tag{6}$$

The Cole-Cole model stress ( $\sigma$ )-strain ( $\epsilon$ ) relation, corresponding to the kernel (1), is

$$\sigma + \tau_\sigma^q \frac{\partial^q \sigma}{\partial t^q} = M_R \left(\epsilon + \tau_\epsilon^q \frac{\partial^q \epsilon}{\partial t^q}\right). \tag{7}$$

The limit  $\tau_\epsilon = 0$  gives the Kelvin-Voigt model implemented in Caputo *et al.* (2011). If  $Q_0 \rightarrow \infty$ , we have the low-frequency elastic limit, with  $\gamma = 1$ ,  $\tau_\epsilon = \tau_\sigma$ , and  $M = M_R$ .

III. PHASE VELOCITY AND QUALITY FACTOR

The complex velocity is the key quantity to obtain the phase velocity and quality factor. In  $n$ -dimensional ( $nD$ ) space, the complex P-wave velocities are

$$\tilde{v}_1(\omega) = \sqrt{\frac{\tilde{K}(\omega) + 2(1 - 1/n)\tilde{\mu}(\omega)}{\rho}}$$

and  $v_1(\omega) = \sqrt{\frac{K_C(\omega) + 2(1 - 1/n)\mu_C(\omega)}{\rho}}, \tag{8}$

where  $\tilde{K}$  and  $\tilde{\mu}$  are the bulk and shear moduli of the thermoelastic medium, respectively,  $K_C$  and  $\mu_C$  are the corresponding Cole-Cole bulk and shear moduli, and  $\rho$  is the composite mass density. Note that in  $nD$  space, the P-wave modulus is  $K_C + 2(1 - 1/n)\mu_C$  [Eq. (3.12) of Carcione (2014)], so that in two-dimensional (2D) space, it is  $K_C + \mu_C$ . This is the value that has to be used in the 2D Green function to obtain the analytical solution to be compared with the 2D numerical simulations.

Similarly, the complex S-wave velocities are

$$\tilde{v}_2(\omega) = \sqrt{\frac{\tilde{\mu}(\omega)}{\rho}} \quad \text{and} \quad v_2(\omega) = \sqrt{\frac{\mu_C(\omega)}{\rho}}. \tag{9}$$

The Cole-Cole phase velocity and quality factor are

$$v_{pi} = \left[\text{Re}\left(\frac{1}{v_i}\right)\right]^{-1}, \quad i = 1(P), 2(S) \tag{10}$$

and

$$Q_i = \frac{\text{Re}(v_i^2)}{\text{Im}(v_i^2)} \tag{11}$$

(e.g., Carcione, 2014). The actual properties of the thermoelastic medium are obtained by replacing  $v_i$  by  $\tilde{v}_i$ .

As stated in Appendix A, pure dilatations do not cause attenuation in Savage’s model, and the main cause is shear deformations (S waves in this case), whose Cole-Cole complex modulus,  $\mu_C$ , is given by Eq. (1) after a fit of  $Q_S$  as a function of frequency, with  $M_R$  given by  $\tilde{\mu}$  [Eq. (A3)]. The bulk modulus is  $K_C = \tilde{K} = \bar{K}$ , with  $\bar{K}$  given by Eq. (A3),

and the complex P-wave modulus can be obtained from Eq. (8) as  $\rho\tilde{v}_1^2$  or as  $\rho v_1^2$ .

#### IV. DYNAMICAL EQUATIONS

The conservation of linear momentum for a 3D linear anelastic medium, describing dilatational and shear deformations, can be written as

$$\rho\partial_t^2 u_i = \partial_j \sigma_{ij}, \quad i, j = 1(x), 2(y), 3(z), \quad (12)$$

where  $\sigma$  and  $u$  denote the stress tensor and the displacement components and  $\partial_t$  and  $\partial_i$  denote the partial time and spatial derivatives, respectively. The initial conditions are  $u_i(0, \mathbf{x}) = 0$ ,  $\partial_t u_i(0, \mathbf{x}) = 0$ , and  $u_i(t, \mathbf{x}) = 0$ , for  $t < 0$ , where  $\mathbf{x} = (x, y, z)$  is the position vector. In the frequency domain, the stress-strain relations can be rewritten as follows:

$$\begin{aligned} \sigma &= \frac{1}{3}(\sigma_{xx} + \sigma_{yy} + \sigma_{zz}) = K(\epsilon_{xx} + \epsilon_{yy} + \epsilon_{zz}) \equiv K\epsilon, \\ \sigma_1 &= \sigma_{xx} - \sigma_{yy} = 2\mu(\epsilon_{xx} - \epsilon_{yy}) \equiv \mu\epsilon_1, \\ \sigma_2 &= \sigma_{xx} - \sigma_{zz} = 2\mu(\epsilon_{xx} - \epsilon_{zz}) \equiv \mu\epsilon_2, \\ \sigma_{xy} &= \mu\epsilon_{xy}, \\ \sigma_{xz} &= \mu\epsilon_{xz}, \\ \sigma_{yz} &= \mu\epsilon_{yz}, \end{aligned} \quad (13)$$

where  $\epsilon$  denotes the strain tensor components, and

$$\begin{aligned} \epsilon_1 &= 2(\epsilon_{xx} - \epsilon_{yy}), \\ \epsilon_2 &= 2(\epsilon_{xx} - \epsilon_{zz}), \\ \epsilon_{ij} &= \partial_i u_j + \partial_j u_i, \end{aligned} \quad (14)$$

where the last equation is the strain-displacement relation.

The above equations correspond to relaxation mechanisms described by the stress-strain relation (7). Then the complete set of equations describing the propagation in three-dimensional (3D) space is

$$\begin{aligned} \partial_t^2 u_i &= \rho^{-1} \partial_j \sigma_{ij}, \\ \sigma + \tau_{\sigma_1}^p \frac{\partial^p \sigma}{\partial t^p} &= K_R \left( \epsilon + \tau_{\epsilon_1}^p \frac{\partial^p \epsilon}{\partial t^p} \right), \\ \sigma_k + \tau_{\sigma_2}^q \frac{\partial^q \sigma_k}{\partial t^q} &= \mu_R \left( \epsilon_k + \tau_{\epsilon_2}^q \frac{\partial^q \epsilon_k}{\partial t^q} \right), \quad k = 1, 2, \\ \sigma_{xy} + \tau_{\sigma_2}^q \frac{\partial^q \sigma_{xy}}{\partial t^q} &= \mu_R \left( \epsilon_{xy} + \tau_{\epsilon_2}^q \frac{\partial^q \epsilon_{xy}}{\partial t^q} \right), \\ \sigma_{xz} + \tau_{\sigma_2}^q \frac{\partial^q \sigma_{xz}}{\partial t^q} &= \mu_R \left( \epsilon_{xz} + \tau_{\epsilon_2}^q \frac{\partial^q \epsilon_{xz}}{\partial t^q} \right), \\ \sigma_{yz} + \tau_{\sigma_2}^q \frac{\partial^q \sigma_{yz}}{\partial t^q} &= \mu_R \left( \epsilon_{yz} + \tau_{\epsilon_2}^q \frac{\partial^q \epsilon_{yz}}{\partial t^q} \right), \end{aligned} \quad (15)$$

where  $p$  and  $q$  refer to the dilatational and shear relaxation mechanisms, respectively, and

$$\begin{aligned} \sigma_{xx} &= \sigma + \frac{1}{3}(\sigma_1 + \sigma_2), \quad \sigma_{yy} = \sigma + \frac{1}{3}(\sigma_2 - 2\sigma_1), \\ \sigma_{zz} &= \sigma + \frac{1}{3}(\sigma_1 - 2\sigma_2). \end{aligned} \quad (16)$$

In 2D space, the above system simplifies as follows:

$$\begin{aligned} \partial_t^2 u_x &= \rho^{-1}(\partial_x \sigma_{xx} + \partial_z \sigma_{xz}), \\ \partial_t^2 u_z &= \rho^{-1}(\partial_x \sigma_{xz} + \partial_z \sigma_{zz}), \\ \sigma + \tau_{\sigma_1}^p \frac{\partial^p \sigma}{\partial t^p} &= K_R \left( \epsilon + \tau_{\epsilon_1}^p \frac{\partial^p \epsilon}{\partial t^p} \right), \\ \bar{\sigma} + \tau_{\sigma_2}^q \frac{\partial^q \bar{\sigma}}{\partial t^q} &= \mu_R \left( \bar{\epsilon} + \tau_{\epsilon_2}^q \frac{\partial^q \bar{\epsilon}}{\partial t^q} \right), \\ \hat{\sigma} + \tau_{\sigma_2}^q \frac{\partial^q \hat{\sigma}}{\partial t^q} &= \mu_R \left( \hat{\epsilon} + \tau_{\epsilon_2}^q \frac{\partial^q \hat{\epsilon}}{\partial t^q} \right), \\ \epsilon &= \partial_x u_x + \partial_z u_z, \\ \bar{\epsilon} &= 2(\partial_x u_x - \partial_z u_z), \\ \hat{\epsilon} &= \partial_x u_z + \partial_z u_x, \end{aligned} \quad (17)$$

where  $\bar{\sigma} = \sigma_2$ ,  $\bar{\epsilon} = \epsilon_2$ ,  $\hat{\sigma} = \sigma_{xz}$ ,  $\hat{\epsilon} = \epsilon_{xz}$  and

$$\sigma_{xx} = \sigma + \frac{1}{2}\bar{\sigma}, \quad \sigma_{zz} = \sigma - \frac{1}{2}\bar{\sigma}. \quad (18)$$

#### V. NUMERICAL ALGORITHM

The fractional derivative is based on the GL approximation (Mainardi, 2010; Podlubny, 1999). The derivative of order  $q$  of a function  $g$  is

$$\frac{\partial^q g}{\partial t^q} \approx D^q g = \frac{1}{h^q} \sum_{j=0}^J (-1)^j \binom{q}{j} g(t - jh), \quad (19)$$

where  $h$  is the time step, and  $J = t/h - 1$ . The derivation of this equation can be found, for instance, in Carcione *et al.* (2002). The fractional derivative of  $g$  at time  $t$  depends on all the previous values of  $g$ . The binomial coefficients are negligible for  $j$  exceeding an integer  $J$ , and this allows us to truncate the sum at  $j=L$ ,  $L \leq J$ , where  $L$  is the effective memory length.

Fractional derivatives of order  $q < 1$  require large memory resources and computational time, because the decay of the binomial coefficients in Eq. (19) is slow (Carcione, 2009; Carcione *et al.*, 2002), and the effective memory length  $L$  is large. We increase the order of the derivative by applying a time derivative of order  $m$  to the third, fourth, and fifth equations of Eq. (17). The result is

$$\begin{aligned} \partial_t^2 u_x &= \rho^{-1}(\partial_x \sigma_{xx} + \partial_z \sigma_{xz}) + f_1, \\ \partial_t^2 u_z &= \rho^{-1}(\partial_x \sigma_{xz} + \partial_z \sigma_{zz}) + f_3, \\ D^m \sigma + \tau_{\sigma_1}^p D^{m+p} \sigma &= K_R \left( D^m \epsilon + \tau_{\epsilon_1}^p D^{m+p} \epsilon \right), \\ D^m \bar{\sigma} + \tau_{\sigma_2}^q D^{m+q} \bar{\sigma} &= \mu_R \left( D^m \bar{\epsilon} + \tau_{\epsilon_2}^q D^{m+q} \bar{\epsilon} \right), \\ D^m \hat{\sigma} + \tau_{\sigma_2}^q D^{m+q} \hat{\sigma} &= \mu_R \left( D^m \hat{\epsilon} + \tau_{\epsilon_2}^q D^{m+q} \hat{\epsilon} \right), \\ \epsilon &= \partial_x u_x + \partial_z u_z, \\ \bar{\epsilon} &= 2(\partial_x u_x - \partial_z u_z), \\ \hat{\epsilon} &= \partial_x u_z + \partial_z u_x, \end{aligned} \quad (20)$$

where we added the source terms  $f_i$  (body forces). It is enough to take  $m = 1$  to have a considerable saving in memory storage compared to  $m = 0$ . We discretize Eq. (20) at  $t = nh$ . Using the notation  $u^n = u(nh)$ , the left-hand side of the first two equations in Eq. (20) can be approximated as

$$h^2(D^2u_i)^n = u_i^{n+1} - 2u_i^n + u_i^{n-1}, \quad i = 1(x), 2(z), \quad (21)$$

where we have used a right-shifted finite-difference expression for the second derivative.

For  $m = 1$ , the GL derivative (19) at time  $nh$  can be rewritten as

$$D^{1+q}g^n = \frac{g^n}{h^{1+q}} + r_g^{(1+q)},$$

$$r_g^{(1+q)} = \frac{1}{h^{1+q}} \sum_{j=1}^J (-1)^j \binom{1+q}{j} g^{n-j}, \quad (22)$$

where  $r_g^{(1+q)}$  has the memory of the field from  $n - 1$  and back in time.

Following Picotti and Carcione (2017), we obtain

$$u_x^{n+1} = h^2 [\rho^{-1}(\partial_x \sigma_{xx} + \partial_z \sigma_{xz}) + f_1] + 2u_x^n - u_x^{n-1},$$

$$u_z^{n+1} = h^2 [\rho^{-1}(\partial_x \sigma_{xz} + \partial_z \sigma_{zz}) + f_3] + 2u_z^n - u_z^{n-1},$$

$$\sigma^n = \frac{1}{a_{\sigma_1}} \left[ \sigma^{n-1} - h\tau_{\sigma_1}^p r_{\sigma}^{1+p} + K_R (a_{\epsilon_1} \epsilon^n - \epsilon^{n-1} + h\tau_{\epsilon_1}^p r_{\epsilon}^{1+p}) \right],$$

$$\bar{\sigma}^n = \frac{1}{a_{\sigma_2}} \left[ \bar{\sigma}^{n-1} - h\tau_{\sigma_2}^q r_{\bar{\sigma}}^{1+q} + \mu_R (a_{\epsilon_2} \bar{\epsilon}^n - \bar{\epsilon}^{n-1} + h\tau_{\epsilon_2}^q r_{\bar{\epsilon}}^{1+q}) \right],$$

$$\hat{\sigma}^n = \frac{1}{a_{\sigma_2}} \left[ \hat{\sigma}^{n-1} - h\tau_{\sigma_2}^q r_{\hat{\sigma}}^{1+q} + \mu_R (a_{\epsilon_2} \hat{\epsilon}^n - \hat{\epsilon}^{n-1} + h\tau_{\epsilon_2}^q r_{\hat{\epsilon}}^{1+q}) \right],$$

$$\epsilon^n = \partial_x u_x^n + \partial_z u_z^n,$$

$$\bar{\epsilon}^n = 2(\partial_x u_x^n - \partial_z u_z^n),$$

$$\hat{\epsilon}^n = \partial_x u_z^n + \partial_z u_x^n, \quad (23)$$

where

$$a_{\xi} = 1 + \left( \frac{\tau_{\xi}}{h} \right)^p, \quad \xi = \epsilon_1, \sigma_1,$$

$$a_{\xi} = 1 + \left( \frac{\tau_{\xi}}{h} \right)^q, \quad \xi = \epsilon_2, \sigma_2. \quad (24)$$

## VI. EXAMPLES

### A. Thermoelastic model

We consider Savage (1966) theory of thermoelasticity for a solid with voids (see Appendix A), which holds for a relatively small porosity, since the voids do not interact (Eshelby, 1957) (e.g.,  $\phi \leq 0.1$ ). Here, we assume an ideal medium with a high thermal expansion coefficient, to obtain a high dissipation, and the following properties:

$$\alpha : 10^{-3} \text{ } ^\circ\text{K}^{-1},$$

$$\gamma/c : 5 \times 10^{-6} \text{ m}^2/\text{s},$$

$$\Gamma = \beta/c : 1.1,$$

$$K/\bar{K} : 1.18,$$

$$\sigma : 0.17,$$

$$K : 39 \text{ GPa} = 39 \times 10^9 \text{ kg}/(\text{m s}^2),$$

$$a : 0.4 \text{ mm} = 0.0004 \text{ m},$$

$$T_0 : 300 \text{ } ^\circ\text{K}, \quad (25)$$

where  $\Gamma$  is the so-called Grüneisen ratio. The porosity and  $\bar{\mu}/\mu$  can be obtained from Eq. (A3), with

$$\phi = \frac{1}{3} \left( \frac{K}{\bar{K}} - 1 \right) \frac{2 - 4\sigma}{1 - \sigma}. \quad (26)$$

We obtain  $\phi = 9.5\%$ ,  $\mu/\bar{\mu} = 1.19$ ,  $\beta = 3\alpha K = 117 \times 10^6 \text{ kg}/(\text{m s}^2 \text{ } ^\circ\text{K})$ ,  $c = \beta/\Gamma = 106 \times 10^6 \text{ kg}/(\text{m s}^2 \text{ } ^\circ\text{K})$ ,  $\gamma = 532 \text{ m kg}/(\text{s}^3 \text{ } ^\circ\text{K})$ ,  $\bar{K} = 33 \text{ GPa}$ ,  $\mu = 33 \text{ GPa}$ ,  $\bar{\mu} = 27.6 \text{ GPa}$ ,  $\bar{\sigma} = 0.173$ , and  $\bar{E} = \bar{K} + 4\bar{\mu}/3 = 70 \text{ GPa}$  [note that  $\mu = 3K(1 - 2\sigma)/(2 + 2\sigma)$ ] (see Appendix A for the definition of the above properties). The composite density is  $\rho = (1 - \phi)\rho_s = 2397$

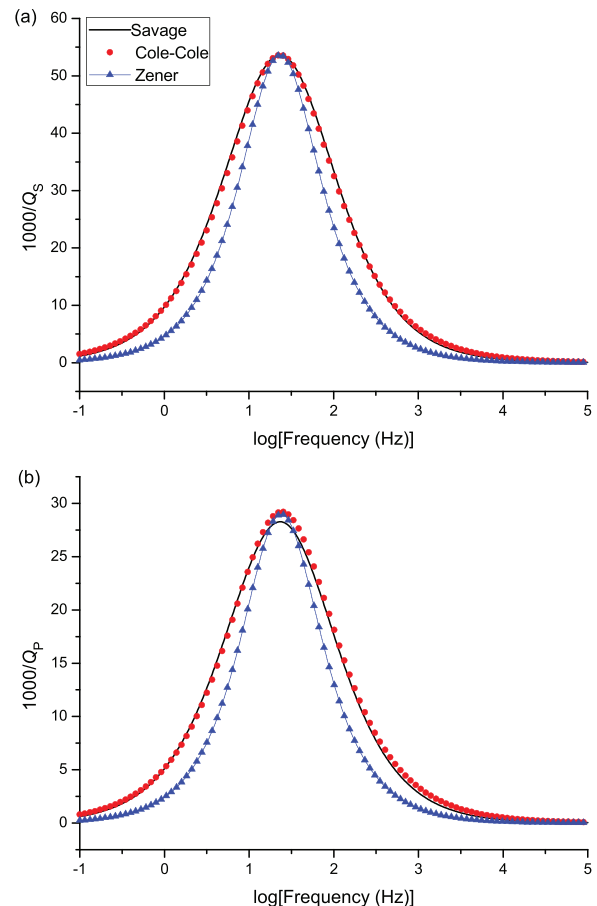


FIG. 1. (Color online) (a) and (b) Dissipation factors of the P and S waves as a function of frequency, with the Cole–Cole ( $q = 0.825$ ) and Zener fits of the shear-wave relaxation peaks.

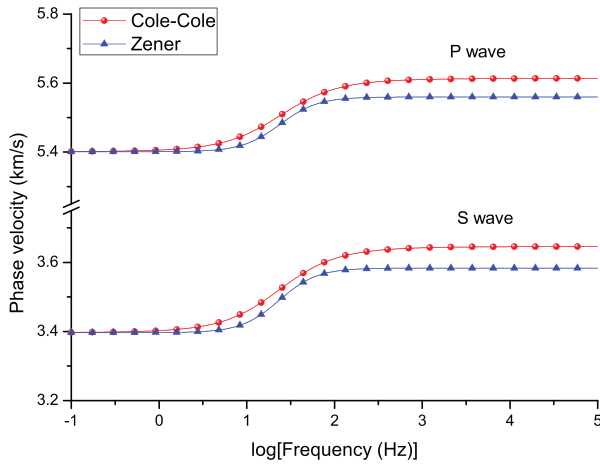


FIG. 2. (Color online) Phase velocities of the P and S waves as a function of frequency, corresponding to the Cole–Cole ( $q=0.825$ ) and Zener models.

$\text{kg/m}^3$ , where  $\rho_s = 2650 \text{ kg/m}^3$  and the 2D relaxed P- and S-wave velocities are 5029 and 3397 m/s, respectively.

In this theory, only shear attenuation occurs [ $K$  is real and  $\mu$  is complex and frequency dependent in Eqs. (8) and (9)], since dilatations are lossless. Then the second equation (15) and the third equation (17) simplify, as well as the

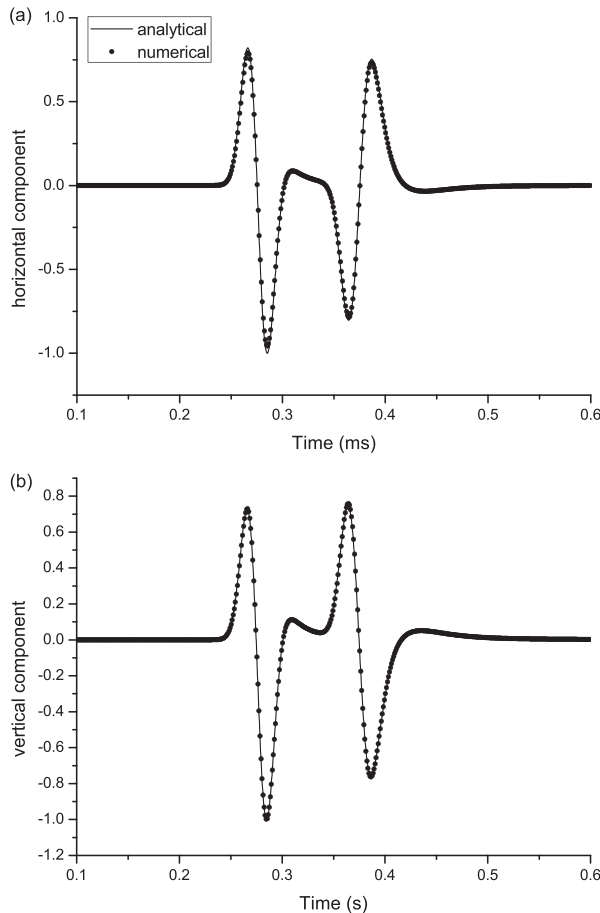


FIG. 3. Comparison between the analytical and numerical solutions of the horizontal and vertical displacements,  $u_x$  (a) and  $u_z$  (b), respectively.

corresponding discrete representations in Eqs. (20) and (23), so that only the fractional order  $q$  is considered. In Eq. (23), we have

$$\sigma^n = \sigma^{n-1} + K_R(\epsilon^n - \epsilon^{n-1}). \quad (27)$$

Figure 1 shows the dissipation factors with the corresponding fits using the Cole–Cole model with  $q=0.825$  and Zener model ( $q=1$ ), where  $f_0=23.37 \text{ Hz}$ ,  $Q_0=18.65$ ,  $\mu_R = \bar{\mu} = 33 \text{ GPa}$ , and  $\mu_U = 36 \text{ GPa}$ .

As can be seen, the Cole–Cole model provides an excellent representation of the physics. The P- and S-wave phase velocities and quality factors are given by Eqs. (10) and (11), respectively, and shown in Fig. 2 for the Cole–Cole and Zener models.

**B. Numerical test**

We verify the algorithm by comparing numerical and analytical solutions for a homogeneous medium (see Appendix B). The source time-history is

$$s(t) = \left(a - \frac{1}{2}\right) \exp(-a), \quad a = \left[\frac{\pi(t - t_s)}{t_p}\right]^2, \quad (28)$$

where  $t_p$  is the period of the wave and we take  $t_s = 1.4t_p$ . Its frequency spectrum is

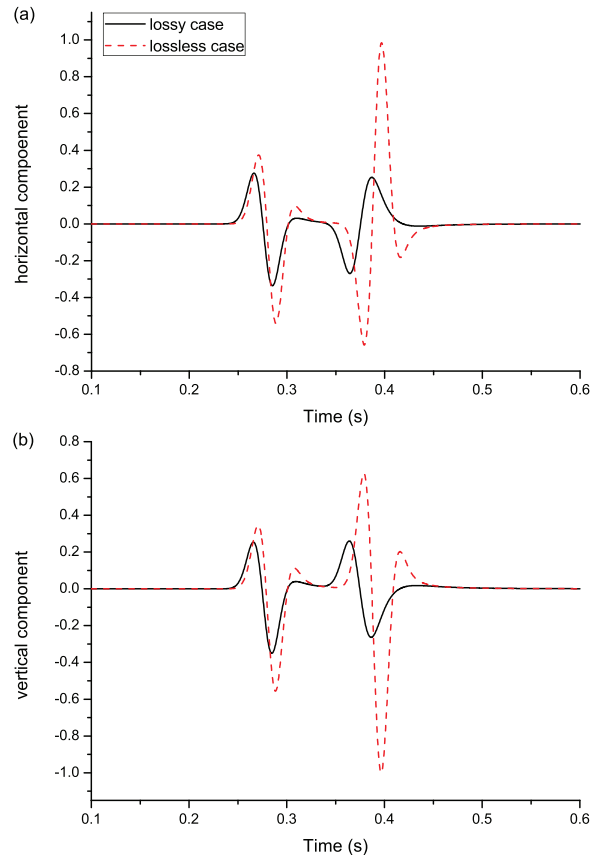


FIG. 4. (Color online) Comparison between the lossless and lossy solutions of the displacements. The lossless case is taken at the zero frequency limit.

$$S(\omega) = \left(\frac{t_p}{\sqrt{\pi}}\right) \bar{a} \exp(-\bar{a} - i\omega t_s),$$

$$\bar{a} = \left(\frac{\omega}{\omega_p}\right)^2, \quad \omega_p = \frac{2\pi}{t_p}, \quad (29)$$

and the peak frequency is  $f_p = 1/t_p$ .

The numerical mesh has uniform vertical and horizontal grid spacings of 20 m and  $231 \times 231$  grid points. The medium properties are those of the previous example. A vertical source is applied at the center of the mesh with a peak frequency equal to the relaxation frequency. We use a memory length  $L = 75$  and a time step  $h = 0.5$  ms. Figure 3 compares the numerical and analytical transient solutions at a distance of  $\sqrt{2} \times 800$  m from the source location.

The agreement between solutions is excellent and has an  $L^2$ -norm error less than 0.5%. Figure 4 compares the elastic (lossless case) with the anelastic case, where the attenuation and velocity dispersion can clearly be appreciated.

Snapshots of the displacements at 0.45 s are displayed in Fig. 5, where the energy radiation pattern can be seen, with the P wave showing maximum energy in the vertical direction and the shear wave along  $45^\circ$  (e.g., Helbig, 1994).

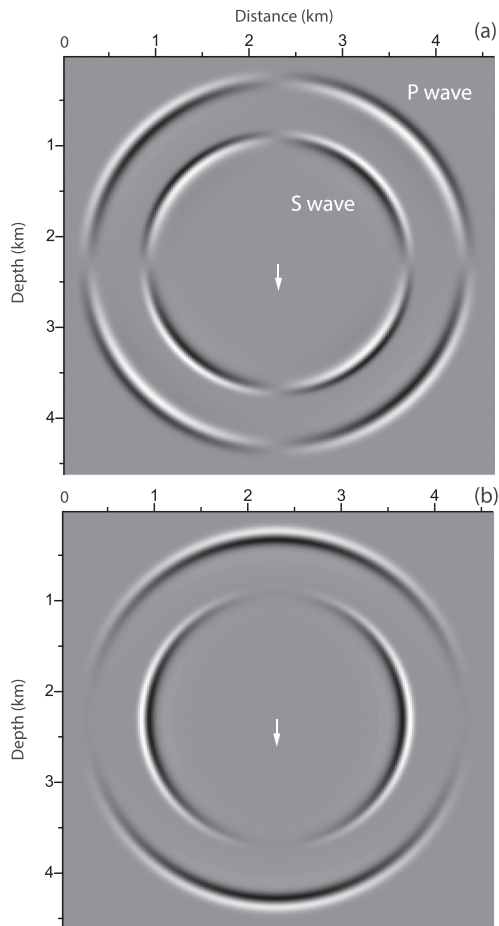


FIG. 5. Snapshots of the displacements,  $u_x$  (a) and  $u_z$  (b) at 0.45 s, due to a vertical force ( $f_3$ ) located at the center of the mesh.

Let us now consider an inhomogeneous medium, specifically, an interface separating two half-spaces. The upper medium has the properties corresponding to the previous examples, while the lower medium has  $K = 147$  GPa,  $\mu = 88$  GPa, and  $\rho = 2650$  Kg/m<sup>3</sup>, and it is lossless. The 2D P- and S-wave velocities are 9428 and 5773 m/s, respectively. Figure 6 shows a snapshot at 0.35 s, where the reflected, transmitted, and refracted events can be observed.

In particular, H denotes the lateral wave connecting the reflected P wavefront with the transmitted P wavefront (e.g., Brekhovskikh, 1960), which is commonly called refracted wave in seismic exploration.

### VII. CONCLUSIONS

We present a numerical algorithm to model thermoelastic wave propagation based on the Cole–Cole model, which implies the solution of fractional time derivatives of stress and strain. This model is better suited to represent thermoelastic peaks than the Zener (or standard linear solid) model. In fact, it is shown that the match between the Cole–Cole model and Savage theory of thermoelasticity is excellent, where this theory describes P- and S-wave propagation and

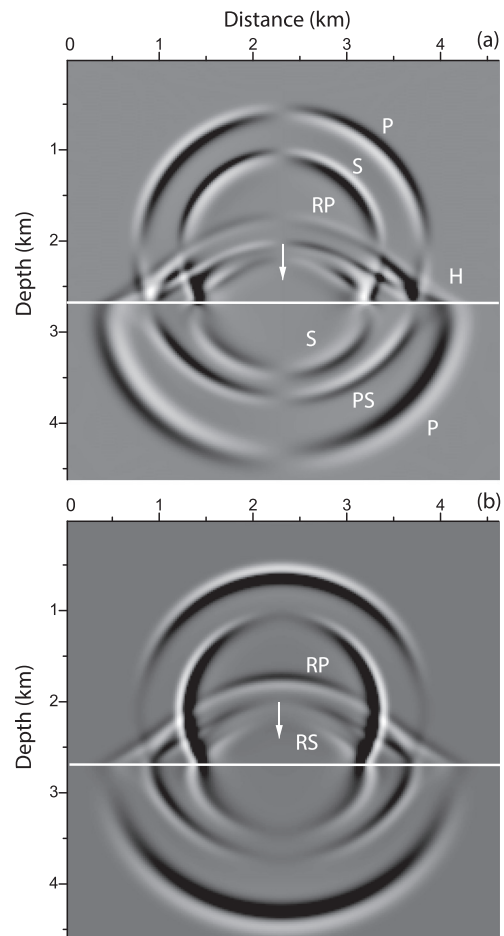


FIG. 6. Snapshots of the displacements,  $u_x$  (a) and  $u_z$  (b) at 0.35 s due to a vertical force ( $f_3$ ) above a medium interface. The P and S waves above and below the interface can be observed. RP, RS, PS, and H denote the reflected P, reflected S, converted PS, and refracted (head) waves.

attenuation in a medium with empty spherical pores. The wave field is computed in the time-space domain using the GL approximation to solve for the fractional derivatives and the Fourier pseudospectral method to calculate the spatial derivatives of the wave equation. The modeling algorithm, which has been tested with the analytical Green's function, can be used to solve wave propagation in general heterogeneous thermoelastic media, as illustrated by an example that considers two half-spaces.

In summary, this work introduces a methodology with two novel aspects: First, the use of a thermoelastic theory to describe attenuation and dispersion and represent the physics with the Cole–Cole model and, second, the simulation of P- and S-wave propagation in the space-time domain using this model. In this way, full-wave synthetic seismograms in general heterogeneous thermoelastic media can be computed.

**ACKNOWLEDGMENTS**

We thank Sven Peter Nasholm, who reviewed the manuscript, for very useful comments. The authors are grateful to the support of the National Natural Science Foundation of China (No. 41974123), the Jiangsu Innovation and Entrepreneurship Plan, China and the Jiangsu Province Science Fund for Distinguished Young Scholars Specially-Appointed.

**APPENDIX A: THERMOELASTIC ATTENUATION BY A MEDIUM WITH SPHERICAL PORES**

Savage (1966) obtained the quality factor of the P and S waves for media filled with spherical voids of radius  $a$ . The P-wave quality factor is

$$Q_P = \frac{3}{2} \times \frac{1 - \bar{\sigma}}{1 - 2\bar{\sigma}} \times Q_S, \tag{A1}$$

where  $Q_S$  is the S-wave quality factor given below and  $\bar{\sigma}$  is the relaxed effective Poisson ratio of the porous medium (at zero frequency), given by

$$\bar{\sigma} = \frac{3\bar{K} - 2\bar{\mu}}{2(3\bar{K} + \bar{\mu})}, \tag{A2}$$

where

$$\bar{K} = \frac{K}{1 + \frac{3\phi(1 - \sigma)}{2 - 4\sigma}}, \quad \bar{\mu} = \frac{\mu}{1 + \frac{15\phi(1 - \sigma)}{7 - 5\sigma}} \tag{A3}$$

(Eshelby, 1957).  $\bar{K}$  and  $\bar{\mu}$  are the relaxed effective bulk and shear moduli of the porous medium [the so-called dry-rock moduli,  $K_R$  and  $\mu_R$  in Eq. (15)];  $\phi$  is the porosity; and  $K$ ,  $\mu$ , and  $\sigma$  are the bulk and shear moduli and Poisson ratio of the solid (or mineral), respectively. For S waves,

$$Q_S^{-1} = \frac{180\mu\phi\Gamma\beta T_0}{\bar{\mu}K} \times \frac{(1 - 2\sigma)(1 + \sigma)}{7 - 5\sigma} \times F(\omega), \tag{A4}$$

where  $T_0$  is a reference absolute temperature for the state of zero stress and strain,  $c$  is the specific heat per unit volume,

$$\beta = (3\lambda + 2\mu)\alpha = 3\alpha K, \tag{A5}$$

$\lambda$  is a Lamé constant,  $\alpha$  is the coefficient of linear thermal expansion (the volumetric one is  $3\alpha$ ) (e.g., Carcione *et al.*, 2019c),

$$F(\omega) = \frac{\chi^2(2\chi^2 + 5\chi + 4)}{\left[ (2\chi^3 - 9\chi - 9)^2 + \chi^2(2\chi^2 + 8\chi + 9)^2 \right]},$$

$$\chi^2 = \frac{\omega c a^2}{2\gamma}, \tag{A6}$$

and  $\gamma$  is the coefficient of heat conduction (or thermal conductivity). The quantities  $\chi$  and  $F$  are dimensionless.

Then the P- and S-wave phase velocities and quality factors are given by Eqs. (10) and (11), respectively, with  $K_C = \bar{K} = \bar{K}$ , since pure dilatations do not cause attenuation, and  $\mu_C$  is given by Eq. (1).

Savage (1966) does not obtain the phase velocity, but strictly, this velocity can be obtained with the method proposed by O'Donnell *et al.* (1981), based on the Kramers–Kronig relations (e.g., Carcione *et al.*, 2019a). Carcione *et al.* (2020a) used this approach to obtain the complex velocity and P-wave modulus of the Savage model. In the present work, it is enough to obtain the Cole–Cole complex modulus by fitting the Savage quality factor, since the Cole–Cole model also obeys the Kramers–Kronig relations.

Thermoelastic attenuation has a peak approximately at the frequency

$$f_0 = \frac{\gamma}{2ca^2}, \tag{A7}$$

where  $\gamma/c$  is a thermal diffusivity and  $\chi^2 = (\pi/2)(f/f_0)$ .

**APPENDIX B: GREEN'S FUNCTION AND ANALYTICAL SOLUTION**

The solution of the wavefield generated by an impulsive point force in a 2D elastic and lossless medium is given by Eason *et al.* (1956) [see also Pilant (1979)]. For a force acting in the positive  $z$ -direction, this solution can be expressed as

$$u_1(r, t) = \left( \frac{F_0}{2\pi\rho} \right) \frac{xz}{r^2} [G_1(r, t) + G_3(r, t)], \tag{B1}$$

$$u_3(r, t) = \left( \frac{F_0}{2\pi\rho} \right) \frac{1}{r^2} [z^2 G_1(r, t) - x^2 G_3(r, t)], \tag{B2}$$

where  $F_0$  is a constant that gives the magnitude of the force,  $r = (x^2 + z^2)^{1/2}$ ,

$$G_1(r, t) = \frac{1}{c_1^2} (t^2 - \tau_P^2)^{-1/2} H(t - \tau_P)$$

$$+ \frac{1}{r^2} (t^2 - \tau_P^2)^{1/2} H(t - \tau_P)$$

$$- \frac{1}{r^2} (t^2 - \tau_S^2)^{1/2} H(t - \tau_S) \tag{B3}$$

and

$$G_3(r, t) = -\frac{1}{c_2^2}(t^2 - \tau_S^2)^{-1/2}H(t - \tau_S) + \frac{1}{r^2}(t^2 - \tau_P^2)^{1/2}H(t - \tau_P) - \frac{1}{r^2}(t^2 - \tau_S^2)^{1/2}H(t - \tau_S), \tag{B4}$$

$$\tau_P = \frac{r}{c_1}, \quad \tau_S = \frac{r}{c_2}, \tag{B5}$$

and  $c_1$  and  $c_2$  are the compressional- and shear-wave phase velocities. To apply the correspondence principle and obtain the anelastic solution, one needs the elastic frequency-domain solution (Bland, 1960; Carcione, 2014). Using the transform pairs of the zero- and first-order Hankel functions of the second kind,

$$\int_{-\infty}^{\infty} \frac{1}{\tau^2}(t^2 - \tau^2)^{1/2}H(t - \tau) \exp(i\omega t) dt = \frac{i\pi}{2\omega\tau} H_1^{(2)}(\omega\tau), \tag{B6}$$

$$\int_{-\infty}^{\infty} (t^2 - \tau^2)^{-1/2}H(t - \tau) \exp(i\omega t) dt = -\frac{i\pi}{2} H_0^{(2)}(\omega\tau), \tag{B7}$$

we obtain

$$u_1(r, \omega, c_1, c_2) = \left(\frac{F_0}{2\pi\rho}\right) \frac{xz}{r^2} [\hat{G}_1(r, \omega, c_1, c_2) + \hat{G}_3(r, \omega, c_1, c_2)], \tag{B8}$$

$$u_3(r, \omega, c_1, c_2) = \left(\frac{F_0}{2\pi\rho}\right) \frac{1}{r^2} [z^2 \hat{G}_1(r, \omega, c_1, c_2) - x^2 \hat{G}_3(r, \omega, c_1, c_2)], \tag{B9}$$

where

$$\hat{G}_1(r, \omega, c_1, c_2) = -\frac{i\pi}{2} \left[ \frac{1}{c_1^2} H_0^{(2)}\left(\frac{\omega r}{c_1}\right) + \frac{1}{\omega r c_2} H_1^{(2)}\left(\frac{\omega r}{c_2}\right) - \frac{1}{\omega r c_1} H_1^{(2)}\left(\frac{\omega r}{c_1}\right) \right], \tag{B10}$$

$$\hat{G}_3(r, \omega, c_1, c_2) = \frac{i\pi}{2} \left[ \frac{1}{c_2^2} H_0^{(2)}\left(\frac{\omega r}{c_2}\right) - \frac{1}{\omega r c_2} H_1^{(2)}\left(\frac{\omega r}{c_2}\right) + \frac{1}{\omega r c_1} H_1^{(2)}\left(\frac{\omega r}{c_1}\right) \right]. \tag{B11}$$

Using the correspondence principle, we replace the elastic wave velocities in Eqs. (B8) and (B9) by the anelastic wave velocities  $v_1$  and  $v_2$  defined in Eqs. (8) and (9). The 2D viscoelastic Green’s function can then be expressed as

$$u_1(r, \omega) = \begin{cases} u_1(r, \omega, v_1, v_2), & \omega \geq 0, \\ u_1^*(r, -\omega, v_1, v_2), & \omega < 0, \end{cases} \tag{B12}$$

and

$$u_3(r, \omega) = \begin{cases} u_3(r, \omega, v_1, v_2), & \omega \geq 0, \\ u_3^*(r, -\omega, v_1, v_2), & \omega < 0, \end{cases} \tag{B13}$$

where the asterisk denotes complex conjugate. This frequency-domain form ensures that the solution is real in the time domain. Multiplication with the source function (29) and a numerical inversion by the discrete Fourier transform yield the desired time-domain solution ( $\hat{G}_1$  and  $\hat{G}_3$  are assumed to be zero at  $\omega = 0$ , since the Hankel functions are singular).

Bagley, R. L., and Torvik, P. J. (1986). “On the fractional calculus model of viscoelastic behavior,” *J. Rheol.* **30**, 133–155.

Bano, M. (2004). “Modelling of GPR waves for lossy media obeying a complex power law of frequency for dielectric permittivity,” *Geophys. Prospect.* **52**, 11–26.

Bland, D. R. (1960). *The Theory of Linear Viscoelasticity* (Pergamon, New York).

Brekhovskikh, L. M. (1960). *Waves in Layered Media* (Academic, London).

Caputo, M. (1967). “Linear models of dissipation whose Q is almost frequency independent—II,” *Geophys. J. Internat.* **13**(5), 529–539.

Caputo, M., Carcione, J. M., and Cavallini, F. (2011). “Wave simulation in biologic media based on the Kelvin–Voigt fractional-derivative stress-strain relation,” *Ultrasound Med. Biol.* **37**, 996–1004.

Caputo, M., and Mainardi, F. (1971). “A new dissipation model based on memory mechanism,” *Pure Appl. Geophys.* **91**(1), 134–147.

Carcione, J. M. (2009). “Theory and modeling of constant-Q P- and S-waves using fractional time derivatives,” *Geophysics* **74**, T1–T11.

Carcione, J. M. (2014). “Handbook of geophysical exploration,” in *Wave Fields in Real Media: Wave Propagation in Anisotropic, Anelastic, Porous and Electromagnetic Media*, 3rd ed. (Elsevier Science, Amsterdam).

Carcione, J. M., Cavallini, F., Ba, J., Cheng, W., and Qadrouh, A. N. (2019a). “On the Kramers–Kronig relations,” *Rheol. Acta* **58**, 21–28.

Carcione, J. M., Cavallini, F., Mainardi, F., and Hanyga, A. (2002). “Time-domain modeling of constant-Q seismic waves using fractional derivatives,” *Pure Appl. Geophys.* **159**, 1719–1736.

Carcione, J. M., Cavallini, F., Wang, E., Ba, J., and Fu, L. Y. (2019b). “Physics and simulation of wave propagation in linear thermo-poroelastic media,” *J. Geophys. Res.* **124**(8), 8147–8166, <https://doi.org/10.1029/2019JB017851>.

Carcione, J. M., Gei, D., Santos, J. E., Fu, L. Y., and Ba, J. (2020a). “Canonical analytical solutions of wave-induced thermoelastic attenuation,” *Geophys. J. Int.* **221**(2), 835–842.

Carcione, J. M., Mainardi, F., Picotti, S., Fu, L. Y., and Ba, J. (2020b). “Thermoelasticity models and P-wave simulation based on the Cole–Cole model,” *J. Therm. Stresses* **43**(4), 1–16.

Carcione, J. M., Wang, Z. W., Ling, W., Salusti, E., Ba, J., and Fu, L. Y. (2019c). “Simulation of wave propagation in linear thermoelastic media,” *Geophysics* **84**(1), T1–T11.

Chandrasekaran, S. N., and Holm, S. (2019). “A multiple relaxation interpretation of the extended Biot model,” *J. Acoust. Soc. Am.* **146**(1), 330–339.

Cole, K. S., and Cole, R. H. (1941). “Dispersion and absorption in dielectrics. I. Alternating current characteristics,” *J. Chem. Phys.* **9**, 341–351.

Eason, J., Fulton, J., and Sneddon, I. N. (1956). “The generation of waves in an infinite elastic solid by variable body forces,” *Philos. Trans. R. Soc. Lond.* **248**(955), 575–607.

Eshelby, J. D. (1957). “The determination of the elastic field of an ellipsoidal inclusion, and related problems,” *Proc. R. Soc. Lond. A* **241**, 376–396.

- Garra, R. (2017). "Propagation of nonlinear thermoelastic waves in porous media within the theory of heat conduction with memory: Physical derivation and exact solutions," *Math. Methods Appl. Sci.* **40**(4), 1307–1315.
- Grimnes, S., and Martinsen, O. G. (2005). "Cole electrical impedance model – A critique and an alternative," *IEEE Trans. Biomed. Eng.* **52**(1), 132–135.
- Hanyga, A. (2003). "An anisotropic Cole–Cole model of seismic attenuation," *J. Comput. Acoust.* **11**(1), 75–90.
- Helbig, K. (1994). *Modeling the Earth for Oil Exploration* (Pergamon, New York).
- Holm, S. (2019). *Waves with Power-Law Attenuation* (Springer, New York).
- Lord, H., and Shulman, Y. (1967). "A generalized dynamical theory of thermoelasticity," *J. Mech. Phys. Solids* **15**(5), 299–309.
- Mainardi, F. (2010). *Fractional Calculus and Waves in Linear Viscoelasticity* (Imperial College Press, London).
- Näsholm, S. P. (2013). "Model-based discrete relaxation process representation of band-limited power-law attenuation," *J. Acoust. Soc. Am.* **133**(3), 1742–1750.
- Näsholm, S. P., and Holm, S. (2013). "On a fractional Zener elastic wave equation," *Fract. Calc. Appl. Anal.* **16**(1), 26–50.
- O'Donnell, M., Jaynes, E. T., and Miller, J. G. (1981). "Kramers-Kronig relationship between ultrasonic-attenuation and phase-velocity," *J. Acoust. Soc. Am.* **69**, 696–701.
- Parker, K., Szabo, T., and Holm, S. (2019). "Towards a consensus on rheological models for elastography in soft tissues," *Phys. Med. Biol.* **64**(21), 215012.
- Picotti, S., and Carcione, J. M. (2017). "Numerical simulation of wave-induced fluid flow seismic attenuation based on the Cole–Cole model," *J. Acoust. Soc. Am.* **142**(1), 134–145.
- Pilant, W. L. (1979). *Elastic Waves in the Earth* (Elsevier, New York).
- Podlubny, I. (1999). *Mathematics in Science and Engineering Fractional Differential Equations: An Introduction to Fractional Derivatives, Fractional Differential Equations, to Methods of Their Solution and Some of Their Applications* (Academic Press, San Diego).
- Savage, J. (1966). "Thermoelastic attenuation of elastic waves by cracks," *J. Geophys. Res.* **71**(16), 3929–3938, <https://doi.org/10.1029/JZ071i016p03929>.
- Spencer, J. W. (1981). "Stress relaxations at low frequencies in fluid-saturated rocks: Attenuation and modulus dispersion," *J. Geophys. Res.* **86**(B3), 1803–1812, <https://doi.org/10.1029/JB086iB03p01803>.
- Treitel, S. (1959). "On the attenuation of small-amplitude plane stress waves in a thermoelastic solid," *J. Geophys. Res.* **64**(6), 661–665, <https://doi.org/10.1029/JZ064i006p00661>.
- Wismer, M. G. (2006). "Finite element analysis of broadband acoustic pulses through inhomogenous media with power law attenuation," *J. Acoust. Soc. Am.* **120**(6), 3493–3502.
- Zener, C. (1938). "Internal friction in solids II. general theory of thermoelastic internal friction," *Phys. Rev.* **53**, 90–99.